Molecular Biology of the Cell
Vol. 21, 1023–1032, March 15, 2010

Regulators of Vps4 ATPase Activity at Endosomes Differentially Influence the Size and Rate of Formation of Intralumenal Vesicles

Daniel P. Nickerson,*† Matthew West,* Ryan Henry,* and Greg Odorizzi*

*Molecular, Cellular and Developmental Biology, University of Colorado, Boulder, CO 80309-0347; and †Department of Biochemistry, University of Washington, Seattle, WA 98195-7350

Submitted September 8, 2009; Revised January 7, 2010; Accepted January 13, 2010
Monitoring Editor: Jean E. Gruenberg

Recruitment of endosomal sorting complexes required for transport (ESCRTs) to the cytosolic face of endosomes regulates selective inclusion of transmembrane proteins into the lumenal vesicles of multivesicular bodies (MVBs). ESCRT-0, -I, and -II bind directly to ubiquitinated transmembrane cargoes of the MVB pathway, whereas polymerization of ESCRT-III at endosomes is thought to bend the membrane and/or provide the energetic force that drives membrane scission and detachment of vesicles into the endosome lumen. Disassembly of the ESCRT-III polymer and dissociation of its subunits from endosomes requires the Vps4 ATPase, the activity of which is controlled in vivo by regulatory proteins. We identify distinct spatiotemporal roles for Vps4-regulating proteins through examinations of subcellular localization and endosome morphology. Did2 plays a unique role in the regulation of MVB lumenal vesicle size, whereas Vtal and Vps60 promote efficient membrane scission and delivery of membrane to the endosome lumen. These morphological effects probably result from Vps4-mediated manipulations of ESCRT-III, because we show dissociation of ESCRT-0, -I, and -II from endosomes is not directly dependent on Vps4 activity.

INTRODUCTION

Transmembrane proteins ubiquitinated on their cytosolic domains are sorted into the lumenal vesicles of multivesicular bodies (MVBs) and are subsequently degraded upon fusion of MVBs with vacuoles/lysosomes. Packaging of ubiquitinated transmembrane protein cargoes into MVB vesicles is mediated by endosomal sorting complexes required for transport (ESCRTs), which are highly conserved and recruited transiently from the cytosol to endosomal membranes (Hurley and Emr, 2006; Williams and Urbe, 2007). ESCRT-0, -I, and -II bind directly to ubiquitinated MVB cargoes (Katzmann *et al*., 2001; Bilodeau *et al*., 2002; Alam *et al*., 2004). In contrast, ESCRT-III consists of four paralogous proteins that assemble on endosomes into a polymer (Babst *et al*., 2002a) that might deform the membrane toward the lumen (Hanson *et al*., 2008) and/or execute vesicle scission (Wollert *et al*., 2009). ESCRT-III also serves as a scaffold for the Bro1-Doa4 deubiquitination machinery that recycles ubiquitin from MVB cargoes before vesicle formation (Luhtala and Odorizzi, 2004).

Dissociation of ESCRTs from endosomes enables repeated rounds of MVB sorting and requires the ATPase Vps4. ATP-bound Vps4 assembles into a double-ring oligomer at endosomes, where it binds directly to ESCRT-III (Babst *et al*., 1998; Yeo *et al*., 2003; Nickerson *et al*., 2006; Obita *et al*., 2007). ATP hydrolysis by Vps4 disassembles ESCRT-III and releases its subunits to the cytosol (Babst *et al*., 2002a). Loss of Vps4 activity not only traps ESCRT-III polymers on endosomes but also prevents dissociation of ESCRT-0, -I, and -II (Katzmann *et al*., 2001; Babst *et al*., 2002b; Bilodeau *et al*., 2002). However, it is unknown whether ESCRT-0, -I, and -II are direct Vps4 substrates, are indirectly dependent on Vps4-mediated disassembly of ESCRT-III, or require another process affected by Vps4.

In vitro studies have characterized five proteins that regulate Vps4 catalytic activity. Vta1 is a positive regulator that binds the catalytic domain of Vps4 (Yeo *et al*., 2003) to promote oligomerization of Vps4 and ATP hydrolysis (Azmi *et al*., 2006; Lottridge *et al*., 2006). Two ESCRT-III paralogues, Did2 and Vps60, are not core subunits of the ESCRT-III polymer but enhance Vta1-mediated stimulation of Vps4 through interactions with the microtubule interaction and transport (MIT) domain of Vta1 (Azmi *et al*., 2008). Did2 and Vps2 (a core ESCRT-III subunit) also stimulate ATP hydrolysis independently of Vta1 through interaction with the MIT domain of Vps4 (Azmi *et al*., 2008). Ist1 counterbalances these positive regulators to inhibit assembly of Vps4 into its active oligomeric state (Dimaano *et al*., 2008).

The functional significance of and coordination among Vps4 regulators in vivo is unknown. To address this issue, we compared ESCRT-III disassembly and endosome morphology in yeast mutants lacking regulators in isolation and in combination. Our results suggest a spatiotemporal separation of Did2 and Vta1-Vps60 functions manifested in distinct phenotypes upon their disruption. ESCRT-III disassembly is more strongly dependent on Did2 than it is on Vta1-Vps60, and the stage at which Did2 promotes Vps4 activity more strongly impacts the size of lumenal vesicles. In contrast, the functions of Vta1 and Vps60 are more closely tied to efficient membrane scission and delivery of vesicles

This article was published online ahead of print in *MBC in Press* (http://www.molbiolcell.org/cgi/doi/10.1091/mbc.E09–09–0776) on January 20, 2010.

Address correspondence to: Greg Odorizzi (odorizzi@colorado.edu).

Abbreviations used: ESCRT, endosomal sorting complex required for transport; MVB, multivesicular bodies; VTE, vesicular tubular endosome.

into the endosome lumen. We further show evidence suggesting that dissociation of ESCRT-0, -I, and -II is not directly mediated by Vps4 activity but instead is dependent upon events leading to normal MVB biogenesis.

MATERIALS AND METHODS

Yeast Strain and Plasmid Construction

Standard protocols were used to construct all yeast strains and plasmids described in Supplemental Table S1 (Longtine *et al.*, 1998).

Microscopy and Imaging

Fluorescence microscopy of cells labeled with *N*-[3-triethylammoniumpropyl]-4-[*p*-diethylaminophenylhexatrienyl] pyridinium dibromide (FM 4-64) was performed as described previously (Luhtala and Odorizzi, 2004). Cryofixation of cells, electron tomography, and three-dimensional modeling has been described previously (Nickerson *et al.*, 2006). Log phase cells were high-pressure frozen and freeze-substituted at −90°C until fixed (Winey *et al.*, 1995; Giddings, 2003) using a Leica automated freeze-substitution (AFS) system. Standard media for tomography and immunolabel was 0.1% uranyl acetate and 0.25% glutaraldehyde in anhydrous acetone. Additional 2% glutaraldehyde was sometimes used to ensure morphological preservation. In brief, samples were warmed in the Leica AFS system from liquid nitrogen temperatures to −90°C and incubated 3 d. Samples were washed in additional anhydrous acetone for a day while warmed to −50°C and then embedded in Lowicryl HM20 over a period of 3 d. Embedded samples were polymerized under UV radiation at −50°C and slowly warmed to room temperature over 4 d. Plastic blocks were sectioned (150–300 nm) on a Leica Ultramicrotome and placed on rhodium-plated copper slot grids with Formvar films. Grids were labeled on both sides with fiducial 15-nm nanogold. Dual tilt series images were collected from +60 to −60° tilt range with 1° increments (Mastronarde, 1997) at 200 kV by using a Tecnai 20 FEG microscope (FEI, Eindhoven, The Netherlands). Tilt series were imaged at 29,000× with a 0.77-nm pixel (binning 2). IMOD and 3dmod software from the 3DEM lab (Kremer *et al.*, 1996) was used for tomogram generation and modeling, respectively. Best-fit sphere models were used to measure diameters of nearly spherical luminal vesicles from the outer leaflet of membrane bilayers. Manually assigned contours of the endosomal limiting membrane at the inner leaflet were used to measure the surface periodically every 3.85 nm and calculated using imodmesh. Digital images were processed using SlideBook (Intelligent Imaging Innovations, Denver, CO) and Photoshop 7.0 (Adobe Systems, Mountain View, CA). Statistical analyses were performed using Prism 4.0 (GraphPad Software, San Diego, CA). Vesicle size and lumenal membrane surface area data were analyzed by analysis of variance (ANOVA) (Newman–Keuls multiple comparison) and *t* tests, respectively. For fluorescence microscopy and electron microscopy (EM) analyses of MVB cargo sorting and endosome morphology summarized in Table 1, a minimum of 100 cells were examined for each genetic background.

Endosomal Sorting Assays, Subcellular Fractionation, Immunoprecipitation, and Western Blotting

Colorimetric plate overlay assays for secretion of the carboxypeptidase Y (CPY)-invertase reporter has been described previously (Darsow *et al.*, 2000). Vacuolar green fluorescent protein (GFP)-cleavage assays were performed by transforming yeast with plasmids encoding GFP-tagged MVB cargo and/or GFP-tagged *VPS60* and growing cells to log phase in selective, synthetic media. Cell pellets were washed in chilled water and precipitated using ice-cold 10% trichloroacetic acid. Protein precipitates were washed in acetone and resuspended in Laemmli sample buffer. SDS-polyacrylamide gel electrophoresis resolved 0.5 OD_{600} unit equivalent of each sample before Western blot analysis. Separation of cell lysates into endosomal membrane pellets and soluble cytosolic fractions has been described previously (Odorizzi *et al.*, 2003). Anti-GFP immunoprecipitations were performed essentially as described previously (Luhtala and Odorizzi, 2004). Antibodies used in Western blotting include polyclonal anti-Vps4 (Babst *et al.*, 1997), polyclonal anti-Snf7 (Babst *et al.*, 1998), polyclonal anti-Vps24 (Babst *et al.*, 1998), monoclonal anti-Por1 (Invitrogen, Carlsbad, CA), monoclonal anti-3-phosphoglycerate kinase (PGK) (Invitrogen), monoclonal anti-Vph1 (Invitrogen), and monoclonal anti-GFP (Roche Diagnostics, Indianapolis, IN). All Western blots were analyzed by chemiluminescence and film exposure except immunoprecipitations of GFP-Did2 and GFP-Vps60 and subcellular fractionations in Figure 2A, which were analyzed using an Odyssey fluorescence scanner (LI-COR Biosciences, Lincoln, NE). Quantifications of relative protein abundance in subcellular fractionation Western blots were performed using Odyssey software (LI-COR Biosciences) and statistically examined by ANOVA (Newman–Keuls multiple comparison) using Prism 4.0 (GraphPad Software).

RESULTS

Vta1 Recruits Vps60 to Endosomes Downstream of Did2-Ist1

Vta1 and Vps60 form a complex at endosomes (Shiflett *et al.*, 2004), interacting with one another via the N-terminal domain of Vta1 (Xiao *et al.*, 2008) and the C-terminal domain of Vps60 (Azmi *et al.*, 2008). Although Vta1 is recruited to endosomes primarily via its interaction with Vps4 (Azmi *et al.*, 2006), Vps60 is recruited to endosomes by interacting with Vta1 (Azmi *et al.*, 2008). We constructed a GFP-Vps60 fusion protein that fully rescued endosomal sorting defects in cells lacking wild-type Vps60 (Supplemental Figure S1). Vps60 in wild-type cells is both cytosolic and associated with multiple, small endosomal puncta, whereas in mutant cells lacking the *VPS4* gene (*vps4*Δ), its cytosolic distribution seems unchanged, but its punctate localization coalesces to fewer and larger structures that correspond to "class E compartments" (Azmi *et al.*, 2008), which are aggregates of endosomes having an aberrant morphology (see below). We observed a striking redistribution of GFP-Vps60 from the cytosol to class E compartments in cells expressing $Vps4^{E233Q}$ (Figure 1A), a catalytically inactive version of Vps4 irreversibly associated with endosomes (Babst *et al.*, 1998). A similar redistribution of Vta1-GFP from the cytosol to class E compartments also occurred in $vps4^{E233Q}$ cells (Figure 1B) but did not in *vps4*Δ cells (Azmi *et al.*, 2006). Thus, endosomal recruitment for Vps60 mirrors that of Vta1 and is promoted by Vps4.

Unlike Vta1 and Vps60, Did2 and Ist1 strongly shift from the cytosol to class E compartments in both *vps4*Δ and $vps4^{E233Q}$ cells (Nickerson *et al.*, 2006; Dimaano *et al.*, 2008). Endosomal recruitment of Did2 is mediated through its interaction with the Vps24 subunit of ESCRT-III (Nickerson *et al.*, 2006) and recruitment of Ist1 occurs through its binding to Did2 (Dimaano *et al.*, 2008; Rue *et al.*, 2008). Although Vta1 is recruited to endosomes primarily through its association with Vps4, the small amount of Vta1 at endosomes in *vps4*Δ cells requires Did2, which directly binds Vta1 (Azmi *et al.*, 2008). Deletion of *DID2* reduced the residual amount of GFP-Vps60 at endosomes in *vps4*Δ cells (data not shown), suggesting recruitment of Vps60 occurs via its interaction with Vta1. Indeed, deletion of *VTA1* strongly reduced endosomal localization of GFP-Vps60 in $vps4^{E233Q}$ cells (Figure 1A), whereas deletion of *VPS60* had no effect on the strong redistribution of Vta1-GFP to class E compartments in $vps4^{E233Q}$ cells (Figure 1B).

Neither Vta1 nor Vps60 were required for endosomal recruitment of GFP-Did2 (Figure 1, C and D) or Ist1-GFP (Rue *et al.*, 2008). Rather, deletion of *VTA1* or *VPS60* enhanced localization of GFP-Did2 at endosomes (Figure 1, C and D), presumably due to reduced stimulation of Vps4 in cells lacking functional Vta1-Vps60 (Azmi *et al.*, 2008). Thus, we conclude Vta1 mediates recruitment of Vps60 to endosomes downstream of ESCRT-III–mediated recruitment of Did2-Ist1.

Vps60 Functions Downstream of Did2 to Promote Vps4-mediated ESCRT-III Disassembly

In vitro, Did2 and Vps60 equally enhance Vta1-mediated stimulation of Vps4 ATPase activity (Azmi *et al.*, 2008), but recruitment of Vps60 downstream of Did2 (Figure 1) suggests their functions might be spatiotemporally distinct. We analyzed the disassembly of ESCRT-III in vivo by subcellular fractionation and found its Vps24 and Snf7 subunits predominantly in the soluble fraction in wild-type cell lysates, which reflects the steady-state balance between mo-

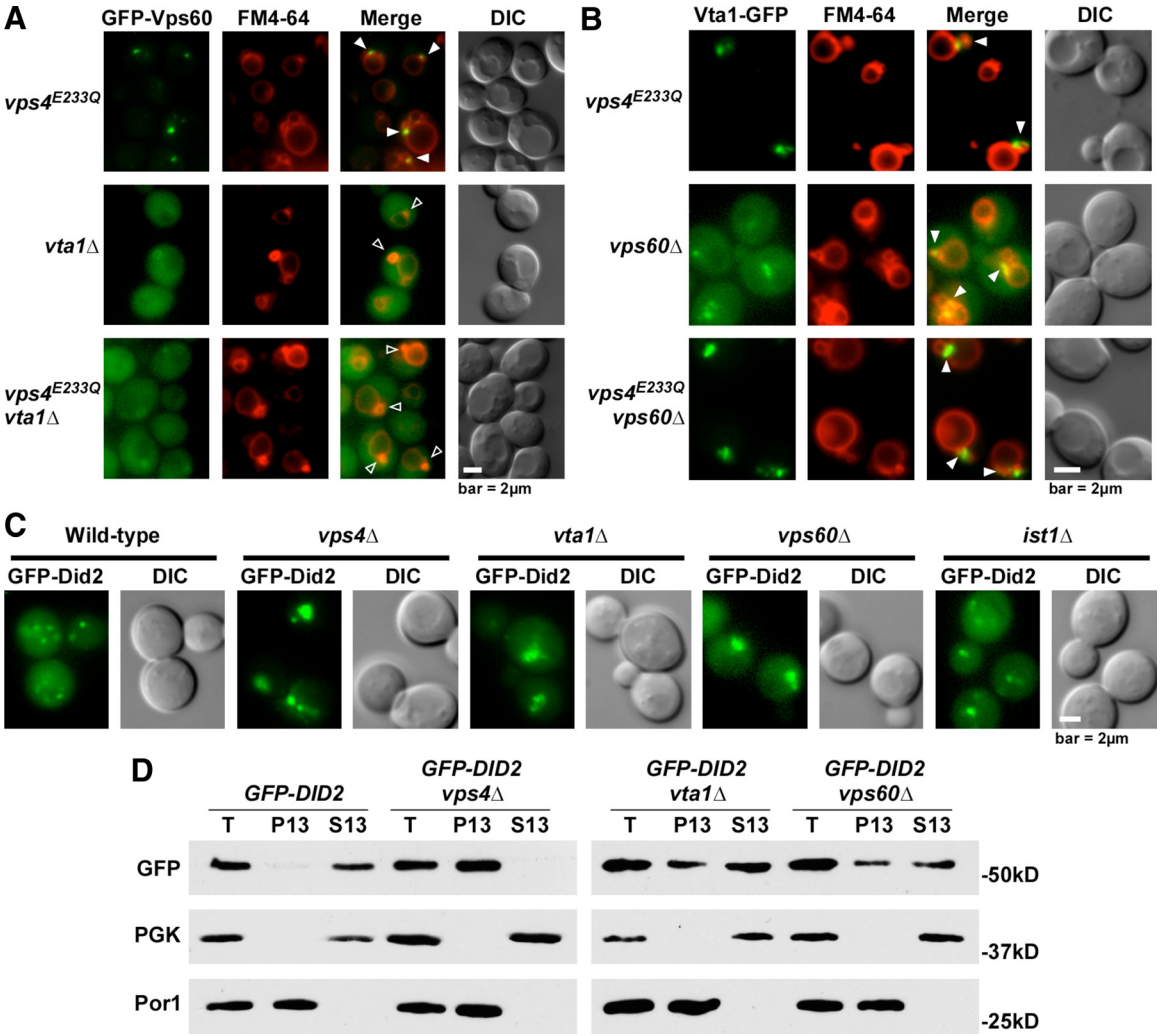

Figure 1. Vta1 recruits Vps60 to endosomes. Fluorescence and differential interference contrast (DIC) microscopy of FM 4-64-stained cells expressing GFP-Vps60 (A) or Vta1-GFP (B), or unstained cells expressing GFP-Did2 (C). Closed arrowheads, colocalization of GFP with FM 4-64; open arrowheads, weak or absent colocalization. Bar, 2 μm. (D) Subcellular fractionation and Western blot analysis of yeast cell lysates. PGK and Por1 (mitochondrial porin) were used as cytosolic and membrane-bound controls, respectively. T, total lysate. P13, membrane-associated 13,000 $\times$ *g* pellet fraction. S13, cytosolic 13,000 $\times$ *g* soluble fraction.

nomeric cytosolic subunits versus subunits assembled into ESCRT-III at endosomes (Babst *et al*., 1998). In contrast, both Vps24 and Snf7 are predominantly membrane-associated in *vps4*Δ cells (Babst *et al*., 1998) and to a lesser extent in *did2*Δ cells, indicating Did2 has a major role in promoting Vps4 activity (Nickerson *et al*., 2006). We found significantly less ESCRT-III to be membrane-associated in *vta1*Δ, *vps60*Δ, and *vta1*Δ *vps60*Δ cells compared with *did2*Δ cells (Figure 2A; one-way ANOVA for Snf7, $p < 0.001$ each). Moreover, significantly less Vps24 and Snf7 remained membrane associated in cells lacking Vta1, Vps60, or both compared with *did2*Δ *vta1*Δ (Figure 2A; Snf7, $p < 0.001$ each; Vps24, $p < 0.05$ each) and *did2*Δ *vps60*Δ cells (Figure 2A; Snf7, $p < 0.001$ each; Vps24, $p < 0.01$ each). These results demonstrate that loss of Did2 function is epistatic to the loss of Vta1 and/or Vps60, signifying that disassembly of ESCRT-III relies more strongly on Vps4 stimulation by Did2 than it does on stimulation by Vta1-Vps60. In addition, *did2*Δ *vta1*Δ and *did2*Δ *vps60*Δ cells accumulated significantly more Snf7 in the membrane-associated fraction compared with *did2*Δ cells (Figure 2A; $p < 0.01$ each), consistent with a synthetic defect in which loss of Did2 and either Vta1 or Vps60 more closely phenocopies loss of Vps4 (Dimaano *et al*., 2008; Rue *et al*., 2008). That Vps24 does not show a similar sensitivity to the loss of both Did2 and either Vta1 or Vps60 might indicate differing requirements for Vps4 regulators in dissociation of the Vps20-Snf7 and Vps2-Vps24 subcomplexes of ESCRT-III.

Fusion of GFP to the C termini of Vps60 or Did2 results in chimeras with compromised function, evidenced by reduced efficiency in dissociation of Snf7 and Vps24 from endosomes (Figure 2B; data not shown). The C termini of ESCRT-III proteins mediate autoinhibitory intramolecular binding to prevent their spurious polymerization and membrane recruitment, and C-terminal fusion of GFP disrupts this autoinhibition, causing the chimeras to accumulate at endosomes (Lin *et al*., 2005; Zamborlini *et al*., 2006; Shim *et al*., 2007). Although subcellular fractionation indicated the characteristic membrane accumulation of both Vps60-GFP (Figure 2B) and Did2-GFP (Nickerson *et al*., 2006) in wild-type cells, we were surprised to find that, unlike Did2-GFP (Nickerson *et al*., 2006), Vps60-GFP shifted to the cytosol in *vps4*Δ cells (Figure 2B). This result demonstrates that even

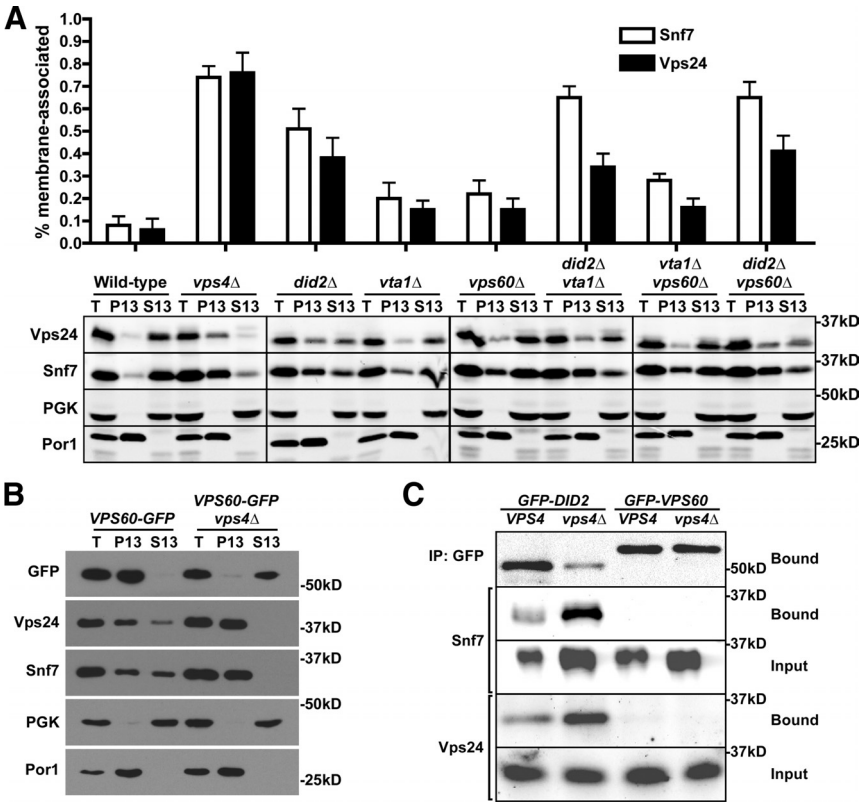

Figure 2. Vps60 functions downstream of Did2 in promoting Vps4-mediated ESCRT-III disassembly. (A and B) Subcellular fractionation and Western blot analysis of yeast cell lysates. Bar graph in A represents quantitative analysis of relative membrane accumulation of Snf7 and Vps24 (n = 4 for all). Mean ± SD. (C) Immunoprecipitations of GFP-Did2 and GFP-Vps60 in the presence and absence of Vps4. T, total lysate. P13, membrane-associated 13,000 × *g* pellet fraction. S13, cytosolic 13,000 × *g* soluble fraction.

when Vps60 is relieved of autoinhibition, its recruitment to endosomes requires Vps4, which underscores the unique status of Vps60 within the ESCRT-III family: whereas Did2 and the core ESCRT-III subunits (Vps20, Snf7, Vps2, and Vps24) localize strongly at endosomes without Vps4 (Babst *et al*., 1998, 2002a; Nickerson *et al*., 2006), Vps60 localizes to endosomes downstream of Vps4 recruitment and is not prone to polymerize with other ESCRT-III family members. Immunoprecipitations of functional, N-terminal GFP chimeras of Did2 and Vps60 reinforce this point. ESCRT-III subunits Snf7 and Vps24 readily copurified with immunoprecipitated Did2 (Figure 2C), and this interaction was enhanced in the absence of Vps4, likely due to polymerization of Did2 and ESCRT-III at the endosome. In contrast, Vps60 pulled down little to no ESCRT-III either in the presence or absence of Vps4. In summary, Did2 plays a more central role in dissociation of ESCRT-III than either Vta1 or Vps60 due to a physical interaction with ESCRT-III that Vta1 and Vps60 do not seem to share in vivo. When we further consider that Did2 bridges interactions between ESCRT-III and Vps4 (Nickerson *et al*., 2006), with the Vps4-stimulator, Vta1 (Lottridge *et al*., 2006), and with the Vps4-inhibitor, Ist1 (Dimaano *et al*., 2008; Xiao *et al*., 2009), the evidence suggests that Did2 occupies a key hub in the management of ESCRT-III dynamics by Vps4.

Distinct Roles for Did2-Ist1 and Vta1-Vps60 in MVB Biogenesis

Unlike spherical MVBs in wild-type cells (Figure 3, A and B; Supplemental Video 1), mutants lacking a functional ESCRT machinery have class E compartments, which are flattened endosomes juxtaposed closely against one another (Rieder *et al*., 1996). Using electron tomography and three-dimensional modeling, we showed previously the absence of lumenal vesicles in class E compartments of *vps4*Δ cells, whereas *did2*Δ cells have crowded, distended endosomes with lumenal vesicles, which we termed "vesicular tubular endosomes," or VTEs (Nickerson *et al*., 2006). The persistence of lumenal vesicles in *did2*Δ cells indicated that efficient disassembly of ESCRT-III is not strictly required for lumenal vesicle budding, a conclusion supported by subsequent in vitro reconstitution of lumenal vesicle formation (Wollert *et al*., 2009). We also observed VTEs in cells lacking the other positive Vps4 regulators, Vta1 and/or Vps60 (Figure 3, C–H, and Supplemental Videos 2–4), whereas cells lacking Ist1 (a negative regulator of Vps4) displayed no defects in general MVB morphology or cargo sorting (Figure 3, I and J, and Supplemental Video 5), suggesting Ist1-mediated inhibition of Vps4 activity is dispensable for MVB function. Nonetheless, deletion of *IST1* or *DID2* strongly exacerbate the morphological and cargo sorting defects in *vta1*Δ and *vps60*Δ cells (Table 1). Simultaneous deletion of both *DID2* and *VTA1* produce the strongest synthetic phenotypes (Table 2), including formation of class E compartments (Figure 3, K and L, and Supplemental Video 6), which reflects the roles of Did2 in recruiting Ist1 (Dimaano *et al*., 2008; Rue *et al*., 2008) and Vta1 in recruiting Vps60 (Figure 1A). In contrast, simultaneous deletion of *DID2* and *IST1* or of *VTA1* and *VPS60* produce no synthetic phenotypes, consistent with Did2-Ist1 and Vta1-Vps60 comprising distinct Vps4 regulatory branches (Dimaano *et al*., 2008; Rue *et al*., 2008). These results are consistent with genetic relationships derived from a previous EM analysis (Rue *et al*., 2008), although improvements in sample preservation and fixation methods allow us to detect lumenal membrane structures to uncover the following morphological distinctions among Did2-Ist1 and Vta1-Vps60 mutants.

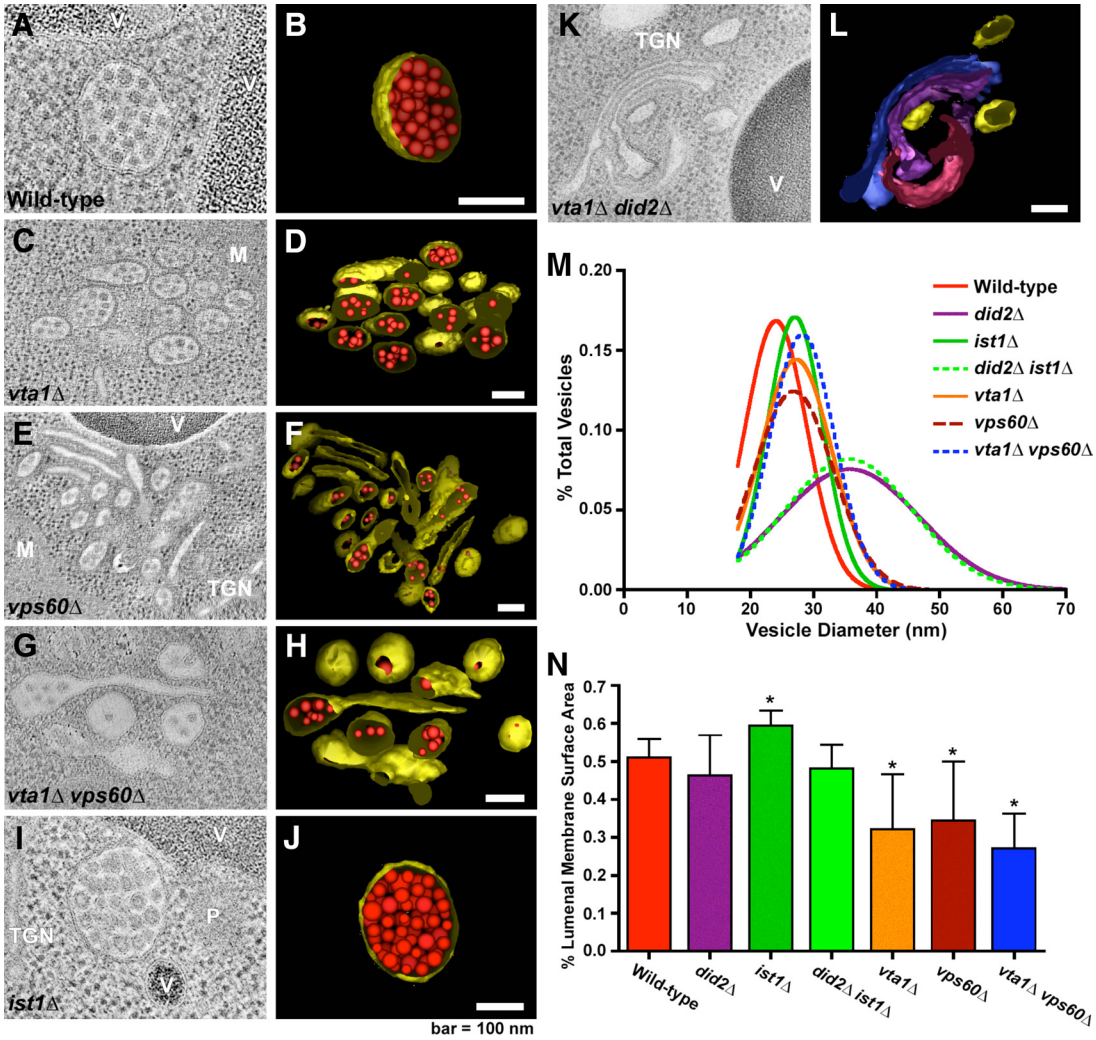

Figure 3. Distinct roles for Did2-Ist1 and Vta1-Vps60 in MVB biogenesis. Two-dimensional cross sections and three-dimensional models from 200-nm-thick section electron tomograms. (A and B) Wild-type MVB. (C and D) *vta1*Δ vesicular tubular endosome (VTE). (E and F) *vps60*Δ VTE with class E compartment cisternae. (G and H) *vta1*Δ *vps60*Δ VTE with isolated flattened membrane. (I and J) *ist1*Δ MVB. (K and L) *did2*Δ *vta1*Δ class E compartment. Endosomal limiting membranes are depicted in yellow, except in the *did2*Δ *vta1*Δ class E compartment in which various colors discriminate discrete membranes. Lumenal vesicles are red. V, vacuole. M, mitochondrion. TGN, *trans*-Golgi network. P, peroxisome. Bar, 100 nm. (M) Distribution of endosomal lumenal vesicle diameters from wild-type, *did2*Δ, *ist1*Δ, *did2*Δ *ist1*Δ, *vta1*Δ, *vps60*, and *vta1*Δ *vps60*Δ cells (n = 295, 369, 176, 113, 525, 362, and 249, respectively). (N) Percentage of total endosome membrane surface area localized to the endosome lumen (n = 11, 4, 8, 4, 6, 5, and 4, respectively). Mean values ± SD. Asterisks indicate statistically significant differences compared with wild type (see text).

The observation of VTEs in cells lacking individual Vps4 regulators indicate neither Did2-Ist1 nor Vta1-Vps60 are strictly required for the formation of lumenal vesicles, but measurement of vesicle sizes in tomographic models revealed differential misregulations of this process. Although lumenal vesicles in wild-type MVBs had a mean diameter of 24 nm (Figure 3M), we found a modest increase (28 nm) in *ist1*Δ, *vta1*Δ, *vps60*Δ, and *vta1*Δ *vps60*Δ mutants (one-way ANOVA; $p < 0.001$ for each). In stark contrast, lumenal vesicles in *did2*Δ and *did2*Δ *ist1*Δ cells were much larger, averaging 36 nm in diameter and frequently ranging above 50 nm (Nickerson *et al*., 2006). This unique swelling in vesicle size suggests the early stage at which Did2 stimulates Vps4 is critical in regulating the timing of membrane scission potentially executed by the ESCRT-III polymer.

We further measured the surface areas of endosome lumenal and limiting membranes to gauge the efficiency of membrane delivery to the endosome lumen. Our selected metric, in which we express lumenal membrane surface area as a share of the total, applies a consistent standard across different endosome diameters and volumes while accommodating variations in limiting membrane topology and lumenal vesicle size. Wild-type MVBs display an equal distribution of surface area between the limiting and lumenal membranes (Figure 3N), but mean lumenal membrane content of endosomes in *vta1*Δ, *vps60*Δ, and *vta1*Δ *vps60*Δ cells fell to 32%, 34 and 27%, respectively (*t* test; $p = 0.0011$, 0.0051, and 0.0001). These reductions occur despite the modest increases in mean vesicle size in these mutants (Figure 3M).

Our interpretation of the quantitative tomographic data considered the possibility that the increased ratio of limiting versus lumenal membrane content arose from a defect in retrograde trafficking from endosomes. A reliable indicator of endosomal retrograde trafficking is Vps10, a transmem-

Table 1. Endosome sorting phenotypes and morphologies

Genetic background	CPY-invertase secretion	GFP-CPS localization	Ub-GFP-CPS localization	Morphology
Wild-type	−	VL[a]	VL	MVB[b]
*vps4*Δ	++	VM[c] + PVC[d]	VM + PVC	Class E[e]
*did2*Δ	−	VM + PVC (VL)[f]	VL + VM + PVC	VTE[g]
*vta1*Δ	−	VL (VM + PVC)	VL	VTE (Class E)
*vps60*Δ	+	VM + PVC (VL)	VL + VM + PVC	VTE (Class E)
*ist1*Δ	−	VL	VL	MVB
*did2*Δ*vta1*Δ	++	VM + PVC	VM + PVC	Class E
*did2*Δ*vps60*Δ	++	VM + PVC	VM + PVC (VL)	Class E (VTE)
*vta1*Δ*vps60*Δ	+	VM + PVC (VL)	VL + VM + PVC	VTE (Class E)
*did2*Δ*ist1*Δ	−	VM + PVC (VL)	VL + VM + PVC	VTE
*vta1*Δ*ist1*Δ	++	VM + PVC	VM + PVC (VL)	Class E (VTE)
*vps60*Δ*ist1*Δ	++	VM + PVC	VM + PVC (VL)	Class E (VTE)

[a] Vacuole lumen, determined by fluorescence microscopy.
[b] Determined by EM.
[c] Vacuole limiting membrane, determined by fluorescence microscopy.
[d] Prevacuolar compartment, determined by fluorescence microscopy.
[e] Class E compartment, determined by EM.
[f] Parentheses indicate uncommon or weak phenotype observed in <20% of cells scored either by fluorescence or EM.
[g] Vesicular tubular endosome, determined by EM.

brane receptor that transports its soluble ligand, CPY, from the Golgi to endosomes, where Vps10 releases CPY and subsequently recycles to the Golgi (Marcusson *et al.*, 1994; Piper *et al.*, 1995). Disruption of the ESCRT machinery traps Vps10 at endosomes, as evidenced by the strong localization of Vps10-GFP at class E compartments in *vps4*Δ cells (Figure 4A). The consequence of Vps10 being unable to recycle from endosomes to the Golgi is the secretion of newly synthesized CPY, which can be detected by expression of a CPY-invertase fusion protein (Figure 4C). In contrast with *vps4*Δ cells, we found that cells lacking Did2, Vta1, or Vps60 exhibit a relatively normal distribution of Vps10-GFP (Figure 4A) and secrete little to no CPY-invertase (Figure 4C), whereas Vps10-GFP is strongly concentrated at class E compartments and CPY-invertase is secreted upon simultaneous disruption of Did2 and Vta1, a condition that phenocopies deletion of *VPS4* with respect to ESCRT-III disassembly (Figure 2) and endosome morphology (Figure 3). Furthermore, although a small fraction of Vps10-GFP is proteolytically cleaved at its lumenal domain in wild-type cells, Vps10-GFP experienced an enhanced degree of cleavage in *vps4*Δ cells (Figure 4B) due to retention at endosomes and the inappropriate maturation of lumenal vacuolar hydrolases at the class E compartment (Babst *et al.*, 2002a). No enrichment of a Vps10 cleavage product was observed in *did2*Δ, *vta1*Δ or *vps60*Δ cells (Figure 4B). Thus, we conclude that the increased ratio of limiting versus lumenal membrane content at endosomes of VTEs in cells lacking Vta1 or Vps60 is derived from a reduction in the budding of lumenal vesicles rather than a defect in recycling of limiting membrane away from endosomes.

In contrast with the above-mentioned mutants lacking positive regulators of Vps4 activity, deletion of *IST1* significantly boosts the lumenal membrane content of endosomes relative to that observed in wild-type cells [61% (*t* test; $p = 0.0009$)]. Although the modest increase in *ist1*Δ vesicle size (Figure 3M) no doubt contributes to this increased lumenal content, *ist1*Δ endosomes routinely seem to have achieved their maximal capacity for lumenal vesicles. Indeed, *ist1*Δ lumenal vesicles frequently occur in apposition to each other and the limiting membrane, potentially pressed together due to lumenal space constraints. Therefore, although our data do not show an increase in the number of *ist1*Δ lumenal vesicles compared with wild type, deletion of *IST1* causes accumulation of vesicles that seems to be limited only by the carrying capacity of the endosome. In *did2*Δ cells and *did2*Δ *ist1*Δ endosomes, we observed no difference in lumenal membrane delivery, suggesting that, whereas absence of Did2 directly impairs Vps4 function, the indirect effect of mislocalizing the negative regulator Ist1 offsets this impairment.

Table 2. Localization of putative Vps4 substrate proteins determined by fluorescence microscopy

	Vps23-GFP ESCRT-I	Vps36-GFP ESCRT-II	GFP-Bro1 N.A.	Doa4-GFP N.A.
Wild-type	Cytosolic[a]	Cytosolic	Cytosolic	Cytosolic
*vps4*Δ	Punctate[b]	Punctate	Punctate	Punctate
*did2*Δ	Cytosolic	Cytosolic	Punctate	Punctate
*vps60*Δ	Cytosolic	Cytosolic	Punctate	Punctate
*vta1*Δ	Cytosolic	Cytosolic	Punctate	Punctate
*vps60*Δ *vta1*Δ	Cytosolic	Cytosolic	Punctate	Punctate
*did2*Δ *vta1*Δ	Punctate	Weak punctate[c]	Punctate	Punctate
*did2*Δ *vps60*Δ	Punctate	Weak punctate	Punctate	Punctate

[a] Predominantly cytosolic GFP signal with occasional weak endosomal puncta.
[b] More intense punctate GFP signal adjacent to the vacuole compared with wild type with a reduction in cytosolic signal.
[c] Weak, punctate GFP signal adjacent to the vacuole without reduction in cytosolic signal.

Endosome Morphology Determines Membrane Association of ESCRT-0, -I, and -II

Original studies of ESCRT-0, -I, and -II reported their accumulation, like ESCRT-III, at class E compartments in *vps4*Δ cells (Katzmann *et al.*, 2001; Babst *et al.*, 2002b; Bilodeau *et al.*, 2002), supporting the broad conclusion that physical manipulation by Vps4 is directly responsible for removal of all

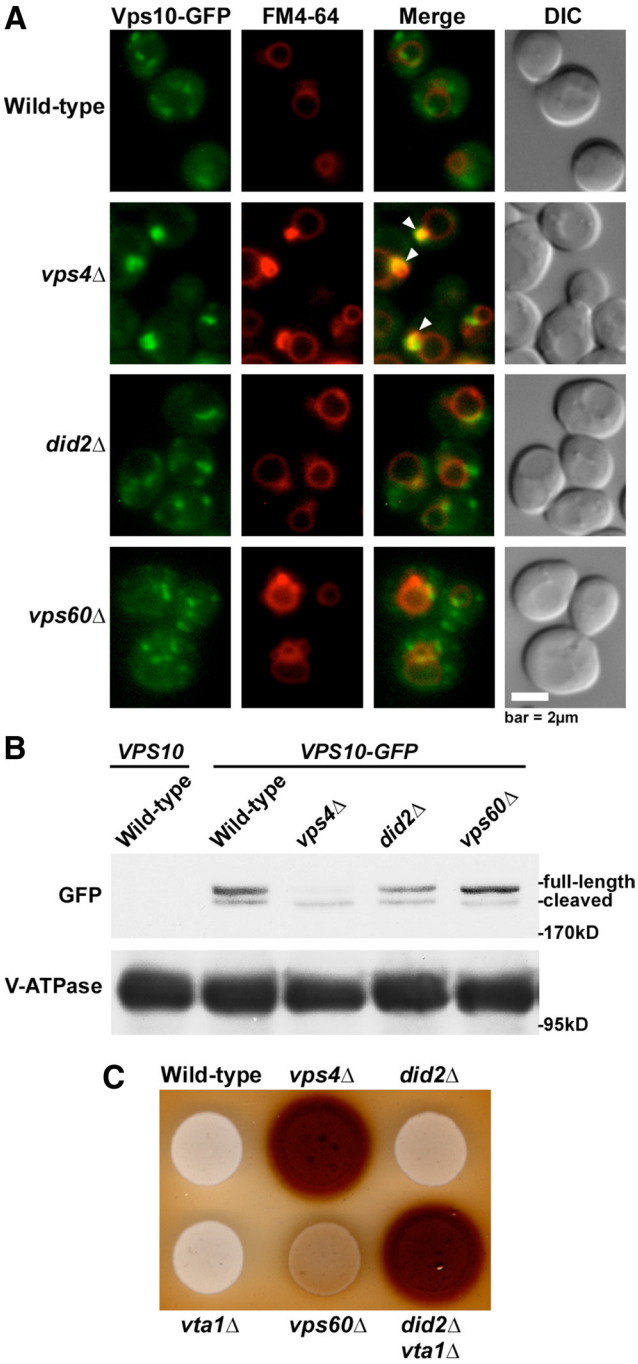

Figure 4. Endosome-to-Golgi retrograde traffic is unperturbed in cells possessing vesicular tubular endosomes. (A) Fluorescence and differential interference contrast (DIC) microscopy of FM 4-64-stained cells expressing Vps10-GFP. Closed arrowheads, colocalization of GFP with FM 4-64; open arrowheads, weak or absent colocalization. Bar, 2 μm. (B) Western blot analysis of yeast cell lysates. V-ATPase (Vph1) was used as a loading control. (C) Colorimetric assay for secretion of CPY-invertase.

ESCRTs from the endosome (Babst *et al*., 2002a; Katzmann *et al*., 2002; Babst, 2005; Hurley and Emr, 2006; Russell *et al*., 2006; Piper and Katzmann, 2007; Williams and Urbe, 2007). However, Vps4 has only been found to bind ESCRT-III. Reporting previously that dissociation of ESCRT-I and -II from endosomes occurs independently of Did2, we speculated that these complexes might require alternative adaptor proteins to be coupled to Vps4 (Nickerson *et al*., 2006). That both Vta1-GFP (Shiflett *et al*., 2004) and GFP-Vps60 (data not shown) lose their ability to localize to endosomes in the absence of ESCRT-I and -II suggested to us that Vta1-Vps60 might serve as the ESCRT-I/-II adaptor. Contrary to this hypothesis, neither Vps23-GFP (ESCRT-I) nor Vps36-GFP (ESCRT-II) accumulate at endosomes in the absence of Vta1, Vps60, or both (Table 2). However, both ESCRT-I and -II are concentrated at endosomes upon simultaneous disruption of Did2 and Vta1-Vps60 functions, conditions under which class E compartments form (Table 1). We therefore explored whether the accumulation of ESCRT-0, -I, and -II at endosomes correlates not with Vps4 malfunction but, instead, with formation of class E compartments by examining *bro1*Δ cells, which have class E compartments indistinguishable from those in *vps4*Δ cells (Richter *et al*., 2007), even though loss of Bro1 causes no aberrant membrane accumulation of ESCRT-III (Odorizzi *et al*., 2003). Hse1-GFP (ESCRT-0), Vps23-GFP and Vps36-GFP all are concentrated at class E compartments in *bro1*Δ cells as strongly as in *vps4*Δ cells (Figure 5A). Importantly, overexpression of the ubiquitin hydrolase encoded by *DOA4* rescues MVB morphology in *bro1*Δ cells (Luhtala and Odorizzi, 2004) and similarly reduces accumulation of Hse1-GFP, Vps23-GFP, and Vps36-GFP at endosomes (Figure 5A). In contrast, *DOA4* overexpression in *vps4*Δ cells fails to reverse the class E compartment morphology (Luhtala and Odorizzi, 2004) nor does it restore the cytosolic distributions of Hse1-GFP, Vps23-GFP, and Vps36-GFP (Figure 5A).

Further indication that "early" ESCRTs (0, I, and II) are not Vps4 substrates comes from our observation that Hse1-GFP, Vps23-GFP, and Vps36-GFP accumulate at endosomes in cells overexpressing *VPS4* (Figure 5B). This condition disrupts vacuolar protein sorting (Kranz *et al*., 2001) but has no apparent effect on Vps4-mediated disassembly of ESCRT-III (Figure 5B), demonstrating that impairment in endosomal dissociation of ESCRT-0, -I, and -II can be uncoupled from ESCRT-III disassembly. Moreover, these data argue against the possibility that ESCRT-III couples Vps4 activity to membrane dissociation of ESCRT-0, -I, and -II. Our conclusion that Vps4 does not directly act toward early ESCRTs to catalyze their membrane dissociation is consistent with failures to detect interactions between Vps4 and the early ESCRTs in systematic studies in metazoans (Martin-Serrano *et al*., 2003; von Schwedler *et al*., 2003) and yeast (Bowers *et al*., 2004).

Because biogenesis of class E compartments in *vps4*Δ, *bro1*Δ, *did2*Δ *vta1*Δ and *did2*Δ *vps60*Δ strains correlates strongly with membrane accumulation of ESCRT-I and -II (Tables 1 and 2), we investigated whether these phenomena share a causative relationship, particularly in light of increasing evidence that early ESCRTs assemble into larger networks on endosome membranes (Hurley, 2008). Class E compartment morphology persists upon simultaneous disruption of ESCRT-I and -II (data not shown), as well as that of ESCRT-0, -I, and -II (Figure 5C). Moreover, class E compartments were also observed upon simultaneous disruption of all four genes encoding the core ESCRT-III subunits (Figure 5D), ruling out the possibility that the ESCRT-III polymer itself drives class E compartment formation. We conclude that accumulation of ESCRTs at endosomes is not directly responsible for the gross morphological defects of class E compartments, rather that class E compartment biogenesis leads to the aberrant endosomal accumulation of ESCRT-0, -I, and -II.

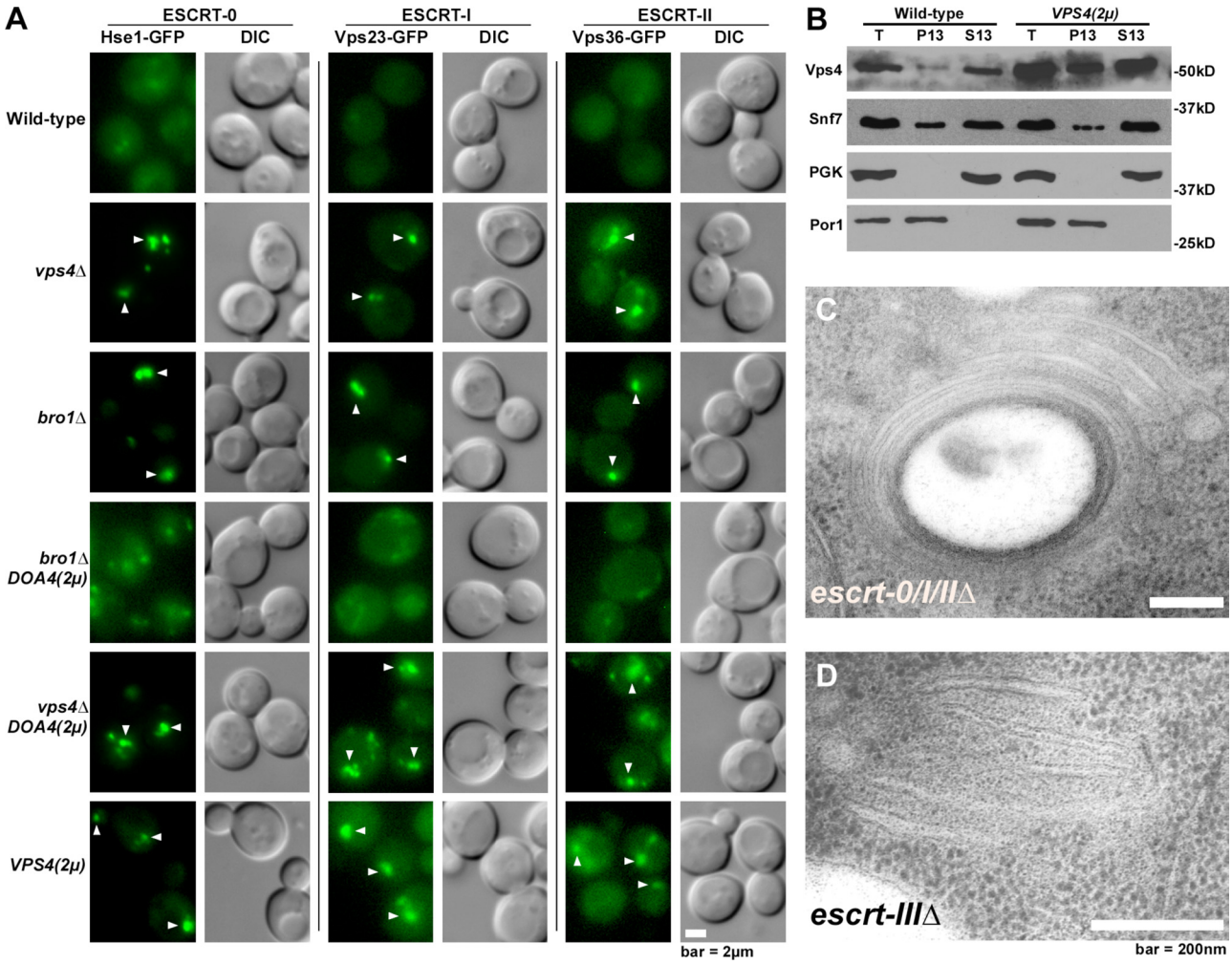

Figure 5. Endosome biogenesis determines membrane association of early ESCRTs. (A) Fluorescence and differential interference contrast (DIC) microscopy of cells expressing Hse1-GFP, Vps23-GFP, or Vps36-GFP. 2μ, overexpression of *DOA4* or *VPS4* from high-copy plasmid. Closed arrowheads indicate localization of GFP to endosomes. Bar, 2 μm. (B) Subcellular fractionation and Western blot analysis of yeast cell lysates. T, total lysate. P13, membrane-associated 13,000 $\times$ *g* pellet fraction. S13, cytosolic 13,000 $\times$ *g* soluble fraction. Thin-section electron micrographs of class E compartments in *vps27*Δ *vps23*Δ *vps36*Δ cells (C) and *vps20*Δ *snf7*Δ *vps2*Δ *vps24*Δ cells (D). Bar, 200 nm.

DISCUSSION

Although in vitro studies have described both positive and negative regulators of Vps4, (Azmi *et al.*, 2008; Dimaano *et al.*, 2008), our in vivo findings point to a spatiotemporal separation of their functions. Cells lacking positive regulators (Did2, Vta1, or Vps60) share phenotypes that include accumulation of ESCRT-III at endosomes (Figure 2A) and formation of VTEs rather than MVBs (Figure 3B). However, electron tomography revealed more subtle phenotypic differences in lumenal vesicle sizes (Figure 3M) and the extent to which lumenal vesicles form (Figure 3N). These observations prompt consideration of whether Vps4 activity toward promoting vesicle formation might not be restricted to one event or moment, but that multiple, distinct manipulations of ESCRT-III might be involved. The spatiotemporal separation between Did2 and Vps60, two proteins with partially redundant capacities to stimulate Vps4 activity (Azmi *et al.*, 2008), makes this scenario especially plausible.

The substantial degree to which dissociation of Vps24 and Snf7 from endosomes occurs in vivo in *vta1*Δ and *vps60*Δ cells (Figure 2A) might reflect the dual capacities of Did2 to stimulate Vps4 both directly and through its interaction with Vta1 (Azmi *et al.*, 2008), which agrees with results from in vitro reconstitution of ESCRT-III disassembly by Vps4 (Davies and Katzmann, personal communication). That Did2 is not strictly dependent on Vta1 to promote Vps4 function in vivo is also consistent with its ability to promote ATP hydrolysis through direct binding to the Vps4 MIT domain (Azmi *et al.*, 2008). Did2 might also influence Vps4 indirectly through interaction with the Vps24-Vps2 subcomplex of ESCRT-III (Nickerson *et al.*, 2006), of which the Vps2 subunit also has the ability in vitro to stimulate Vps4 activity independently of Vta1 (Azmi *et al.*, 2008). In contrast to Did2, Vps60 might rely exclusively on Vta1 to promote Vps4 function. Indeed, Vta1 is the only known binding partner for Vps60 in yeast (Shiflett *et al.*, 2004) and metazoans (Ward *et al.*, 2005). Did2, therefore, plays a more central role in management of ESCRT-III dissociation than either Vta1 or Vps60.

A distinct role for Did2 is also evident when comparing endosomal morphologies. Cells lacking Did2 display a unique increase in vesicle size not shared by cells lacking other Vps4 regulators (Figure 3M). The more pronounced defect in ESCRT-III membrane dissociation seen in *did2*Δ

cells compared with *vta1*Δ and *vps60*Δ cells (Figure 2A) suggests the swelled vesicle phenotype results either from misregulated manipulation of ESCRT-III by Vps4 at the moment of vesicle scission or from reduced availability of recycled ESCRT-III subunits capable of assembling to mediate repeated rounds of vesicle budding. We note, however, that ESCRT-III has been recently shown in vitro to perform its membrane scission function in the absence of Vps4 (Wollert *et al*., 2009). Therefore, considering the capacity of Did2 (and the incapacity of Vps60) to bind the ESCRT-III core complex (Figure 2C), we should also consider the possibility that Did2 might regulate vesicle scission not only through regulation of Vps4, but also through direct participation in the ESCRT-III polymer.

Insight into the relationship between endosome morphology and MVB cargo sorting can be gleaned by comparison of the phenotypes exhibited by *vta1*Δ cells. Despite having VTEs with reduced lumenal membrane content (Figure 3), *vta1*Δ cells display only very weak MVB cargo sorting defects across a battery of MVB cargo proteins (Table 1 and Supplemental Figure S1). This lack of correlation suggests that the 40% reduction in bulk lumenal membrane sorting is insufficient to disrupt MVB cargo sorting and that MVB vesicles typically form without having achieved cargo saturation. Considering the recent discovery that separate disruptions of ubiquitin-binding by either ESCRT-I or -II are insufficient to impair MVB cargo sorting (Shields *et al*., 2009), it also seems that ESCRT-mediated cargo recognition typically operates well short of saturation. These insights are consistent with the proposition that endosome lumenal vesicle formation and cargo selection are not strictly interdependent. Indeed, loss of Rsp5 or Doa4 severely disrupts MVB cargo ubiquitination and sorting (Katzmann *et al*., 2004; Luhtala and Odorizzi, 2004) without disrupting MVB biogenesis (McNatt *et al*., 2007; Richter *et al*., 2007). Although an urgent need to silence and degrade cargoes can result in physiological stimulation of vesicle budding (White *et al*., 2006), it seems that lumenal vesicle formation is largely "hard-wired" to occur with or without cargo.

Given that *did2*Δ and *vps60*Δ endosomes suffer no greater impairment in lumenal membrane delivery than *vta1*Δ endosomes (Figure 3), it seems that the more significant MVB cargo sorting defects observed in *did2*Δ and *vps60*Δ cells (Table 1 and Supplemental Figure S1) do not result from insufficient lumenal membrane carrying capacity, rather from disruptions to ESCRT-III dynamics that are not shared by *vta1*Δ. This highlights an ongoing conundrum in understanding the Vta1-Vps60 relationship: how is it that loss of Vps60, the clearest function of which is stimulation of Vps4 through interaction with Vta1 (Azmi *et al*., 2008), produces consistently stronger cargo missorting phenotypes than does loss of Vta1? At this point, genetic evidence suggests Vps60 performs a secondary, Vta1-independent function, but given the lack of interaction between Vps60 and the other ESCRT-III family proteins (Figure 2), it is unclear what this role is.

Recent studies of ESCRT-III have demonstrated the ability of its core subunits, especially Snf7, to polymerize at membranes in spiral patterns that might serve to induce membrane curvature (Hanson *et al*., 2008; Lata *et al*., 2008; Saksena *et al*., 2009). Observing also the ability of the Vps20-Snf7 subcomplex to protect MVB cargoes from proteolytic cleavage (Babst *et al*., 2002a) and prevent recycling of MVB cargoes away from endosomes (Teis *et al*., 2008), current opinion favors a model in which ESCRT-III forms a corral to prevent lateral diffusion of cargoes away from the membrane domain that will form a vesicle. Although most MVB cargoes examined show only partial missorting in *did2*Δ and *vps60*Δ cells (Dimaano *et al*., 2008; Rue *et al*., 2008), these mutants both display a complete block in vacuolar trafficking of the a-factor mating receptor Ste3 (Supplemental Figure S1). Given the inefficient membrane dissociation of ESCRT-III in *did2*Δ and *vps60*Δ mutants (Figure 2), this might suggest a failure to corral Ste3 to ensure its lumenal targeting. However, we note that MVB trafficking of another endocytic cargo with rapid endosome recycling kinetics, Mup1, is unperturbed in *did2*Δ cells (Teis *et al*., 2008), suggesting that defective ESCRT-III assembly kinetics do not provide a sufficient explanation for cargo missorting in *did2*Δ and *vps60*Δ mutants. Interestingly, fusion of a nonhydrolyzable, in-frame ubiquitin to the cytosolic domain of carboxypeptidase S substantially rescues MVB sorting in all single mutants and combinations of *did2*Δ, *vta1*Δ, and *vps60*Δ capable of forming lumenal vesicles (Table 1), indicating a possible alternative scenario involving misregulation of the Bro1-Doa4 deubiquitination machinery that accumulates at VTEs along with ESCRT-III (Table 2).

ACKNOWLEDGMENTS

We thank Caitlin White-Root, Caleb Richter, and Michael Kaempf (University of Colorado–Boulder) for yeast strains; Alex Merz (University of Washington) for generously providing resources and space to perform experiments; Matthew Russell (University of Colorado–Boulder) for EM assistance; and Andrew Staehelin (University of Colorado–Boulder), Ishara Azmi, Brian Davies, and David Katzmann (Mayo Clinic, Rochester, MN) for discussion of unpublished results. This work was funded by National Institutes of Health grant GM-065505.

REFERENCES

Alam, S. L., Sun, J., Payne, M., Welch, B. D., Blake, B. K., Davis, D. R., Meyer, H. H., Emr, S. D., and Sundquist, W. I. (2004). Ubiquitin interactions of NZF zinc fingers. EMBO J. *23*, 1411–1421.

Azmi, I., Davies, B., Dimaano, C., Payne, J., Eckert, D., Babst, M., and Katzmann, D. J. (2006). Recycling of ESCRTs by the AAA-ATPase Vps4 is regulated by a conserved VSL region in Vta1. J. Cell Biol. *172*, 705–717.

Azmi, I. F., Davies, B. A., Xiao, J., Babst, M., Xu, Z., and Katzmann, D. J. (2008). ESCRT-III family members stimulate Vps4 ATPase activity directly or via Vta1. Dev. Cell *14*, 50–61.

Babst, M. (2005). A protein's final ESCRT. Traffic *6*, 2–9.

Babst, M., Katzmann, D. J., Estepa-Sabal, E. J., Meerloo, T., and Emr, S. D. (2002a). Escrt-III: an endosome-associated heterooligomeric protein complex required for mvb sorting. Dev. Cell *3*, 271–282.

Babst, M., Katzmann, D. J., Snyder, W. B., Wendland, B., and Emr, S. D. (2002b). Endosome-associated complex, ESCRT-II, recruits transport machinery for protein sorting at the multivesicular body. Dev Cell *3*, 283–289.

Babst, M., Sato, T. K., Banta, L. M., and Emr, S. D. (1997). Endosomal transport function in yeast requires a novel AAA-type ATPase, Vps4p. EMBO J. *16*, 1820–1831.

Babst, M., Wendland, B., Estepa, E. J., and Emr, S. D. (1998). The Vps4p AAA ATPase regulates membrane association of a Vps protein complex required for normal endosome function. EMBO J. *17*, 2982–2993.

Bilodeau, P. S., Urbanowski, J. L., Winistorfer, S. C., and Piper, R. C. (2002). The Vps27p Hse1p complex binds ubiquitin and mediates endosomal protein sorting. Nat. Cell Biol. *4*, 534–539.

Bowers, K., Lottridge, J., Helliwell, S. B., Goldthwaite, L. M., Luzio, J. P., and Stevens, T. H. (2004). Protein-protein interactions of ESCRT complexes in the yeast *Saccharomyces cerevisiae*. Traffic *5*, 194–210.

Darsow, T., Odorizzi, G., and Emr, S. D. (2000). Invertase fusion proteins for analysis of protein trafficking in yeast. Methods Enzymol. *327*, 95–106.

Dimaano, C., Jones, C. B., Hanono, A., Curtiss, M., and Babst, M. (2008). Ist1 regulates Vps4 localization and assembly. Mol. Biol. Cell *19*, 465–474.

Giddings, T. H. (2003). Freeze-substitution protocols for improved visualization of membranes in high-pressure frozen samples. J. Microsc. *212*, 53–61.

Hanson, P. I., Roth, R., Lin, Y., and Heuser, J. E. (2008). Plasma membrane deformation by circular arrays of ESCRT-III protein filaments. J. Cell Biol. *180*, 389–402.

Hurley, J. H. (2008). ESCRT complexes and the biogenesis of multivesicular bodies. Curr. Opin. Cell Biol. *20*, 4–11.

Hurley, J. H., and Emr, S. D. (2006). The ESCRT complexes: structure and mechanism of a membrane-trafficking network. Annu. Rev. Biophys. Biomol. Struct. *35*, 277–298.

Katzmann, D. J., Babst, M., and Emr, S. D. (2001). Ubiquitin-dependent sorting into the multivesicular body pathway requires the function of a conserved endosomal protein sorting complex, ESCRT-I. Cell *106*, 145–155.

Katzmann, D. J., Odorizzi, G., and Emr, S. D. (2002). Receptor downregulation and multivesicular-body sorting. Nat. Rev. Mol. Cell Biol. *3*, 893–905.

Katzmann, D. J., Sarkar, S., Chu, T., Audhya, A., and Emr, S. D. (2004). Multivesicular body sorting: ubiquitin ligase Rsp5 is required for the modification and sorting of carboxypeptidase S. Mol. Biol. Cell *15*, 468–480.

Kranz, A., Kinner, A., and Kolling, R. (2001). A family of small coiled-coil-forming proteins functioning at the late endosome in yeast. Mol. Biol. Cell *12*, 711–723.

Kremer, J. R., Mastronarde, D. N., and McIntosh, J. R. (1996). Computer visualization of three-dimensional image data using IMOD. J. Struct. Biol. *116*, 71–76.

Lata, S., Schoehn, G., Jain, A., Pires, R., Piehler, J., Gottlinger, H. G., and Weissenhorn, W. (2008). Helical structures of ESCRT-III are disassembled by VPS4. Science *321*, 1354–1357.

Lin, Y., Kimpler, L. A., Naismith, T. V., Lauer, J. M., and Hanson, P. I. (2005). Interaction of the mammalian endosomal sorting complex required for transport (ESCRT) III protein hSnf7–1 with itself, membranes, and the AAA+ ATPase SKD1. J. Biol. Chem. *280*, 12799–12809.

Longtine, M. S., McKenzie, A., 3rd, Demarini, D. J., Shah, N. G., Wach, A., Brachat, A., Philippsen, P., and Pringle, J. R. (1998). Additional modules for versatile and economical PCR-based gene deletion and modification in *Saccharomyces cerevisiae*. Yeast *14*, 953–961.

Lottridge, J. M., Flannery, A. R., Vincelli, J. L., and Stevens, T. H. (2006). Vta1p and Vps46p regulate the membrane association and ATPase activity of Vps4p at the yeast multivesicular body. Proc. Natl. Acad. Sci. USA *103*, 6202–6207.

Luhtala, N., and Odorizzi, G. (2004). Bro1 coordinates deubiquitination in the multivesicular body pathway by recruiting Doa4 to endosomes. J. Cell Biol. *166*, 717–729.

Marcusson, E. G., Horazdovsky, B. F., Cereghino, J. L., Gharakhanian, E., and Emr, S. D. (1994). The sorting receptor for yeast vacuolar carboxypeptidase Y is encoded by the VPS10 gene. Cell *77*, 579–586.

Martin-Serrano, J., Yarovoy, A., Perez-Caballero, D., and Bieniasz, P. D. (2003). Divergent retroviral late-budding domains recruit vacuolar protein sorting factors by using alternative adaptor proteins. Proc. Natl. Acad. Sci. USA *100*, 12414–12419.

Mastronarde, D. N. (1997). Dual-axis tomography: an approach with alignment methods that preserve resolution. J. Struct. Biol. *120*, 343–352.

McNatt, M. W., McKittrick, I., West, M., and Odorizzi, G. (2007). Direct binding to Rsp5 mediates ubiquitin-independent sorting of Sna3 via the multivesicular body pathway. Mol. Biol. Cell *18*, 697–706.

Nickerson, D. P., West, M., and Odorizzi, G. (2006). Did2 coordinates Vps4-mediated dissociation of ESCRT-III from endosomes. J. Cell Biol. *175*, 715–720.

Obita, T., Saksena, S., Ghazi-Tabatabai, S., Gill, D. J., Perisic, O., Emr, S. D., and Williams, R. L. (2007). Structural basis for selective recognition of ESCRT-III by the AAA ATPase Vps4. Nature *449*, 735–739.

Odorizzi, G., Katzmann, D. J., Babst, M., Audhya, A., and Emr, S. D. (2003). Bro1 is an endosome-associated protein that functions in the MVB pathway in *Saccharomyces cerevisiae*. J. Cell Sci. *116*, 1893–1903.

Piper, R. C., Cooper, A. A., Yang, H., and Stevens, T. H. (1995). VPS27 controls vacuolar and endocytic traffic through a prevacuolar compartment in *Saccharomyces cerevisiae*. J. Cell Biol. *131*, 603–617.

Piper, R. C., and Katzmann, D. J. (2007). Biogenesis and function of multivesicular bodies. Annu. Rev. Cell Dev. Biol. *23*, 519–547.

Richter, C., West, M., and Odorizzi, G. (2007). Dual mechanisms specify Doa4-mediated deubiquitination at multivesicular bodies. EMBO J. *26*, 2454–2464.

Rieder, S. E., Banta, L. M., Kohrer, K., McCaffery, J. M., and Emr, S. D. (1996). Multilamellar endosome-like compartment accumulates in the yeast vps28 vacuolar protein sorting mutant. Mol. Biol. Cell *7*, 985–999.

Rue, S. M., Mattei, S., Saksena, S., and Emr, S. D. (2008). Novel Ist1-Did2 complex functions at a late step in multivesicular body sorting. Mol. Biol. Cell *19*, 475–484.

Russell, M. R., Nickerson, D. P., and Odorizzi, G. (2006). Molecular mechanisms of late endosome morphology, identity and sorting. Curr. Opin. Cell Biol. *18*, 422–428.

Saksena, S., Wahlman, J., Teis, D., Johnson, A. E., and Emr, S. D. (2009). Functional reconstitution of ESCRT-III assembly and disassembly. Cell *136*, 97–109.

Shields, S. B., Oestreich, A. J., Winistorfer, S., Nguyen, D., Payne, J. A., Katzmann, D. J., and Piper, R. (2009). ESCRT ubiquitin-binding domains function cooperatively during MVB cargo sorting. J. Cell Biol. *185*, 213–224.

Shiflett, S. L., Ward, D. M., Huynh, D., Vaughn, M. B., Simmons, J. C., and Kaplan, J. (2004). Characterization of Vta1p, a class E Vps protein in *Saccharomyces cerevisiae*. J. Biol. Chem. *279*, 10982–10990.

Shim, S., Kimpler, L. A., and Hanson, P. I. (2007). Structure/function analysis of four core ESCRT-III proteins reveals common regulatory role for extreme C-terminal domain. Traffic *8*, 1068–1079.

Teis, D., Saksena, S., and Emr, S. D. (2008). Ordered assembly of the ESCRT-III complex on endosomes is required to sequester cargo during MVB formation. Dev. Cell *15*, 578–589.

von Schwedler, U. K., *et al*. (2003). The protein network of HIV budding. Cell *114*, 701–713.

Ward, D. M., Vaughn, M. B., Shiflett, S. L., White, P. L., Pollock, A. L., Hill, J., Schnegelberger, R., Sundquist, W. I., and Kaplan, J. (2005). The role of LIP5 and CHMP5 in multivesicular body formation and HIV-1 budding in mammalian cells. J. Biol. Chem. *280*, 10548–10555.

White, I. J., Bailey, L. M., Aghakhani, M. R., Moss, S. E., and Futter, C. E. (2006). EGF stimulates annexin 1-dependent inward vesiculation in a multivesicular endosome subpopulation. EMBO J. *25*, 1–12.

Williams, R. L., and Urbe, S. (2007). The emerging shape of the ESCRT machinery. Nat. Rev. Mol. Cell Biol. *8*, 355–368.

Winey, M., Mamay, C. L., O'Toole, E. T., Mastronarde, D. N., Giddings, T. H., Jr., McDonald, K. L., and McIntosh, J. R. (1995). Three-dimensional ultrastructural analysis of the *Saccharomyces cerevisiae* mitotic spindle. J. Cell Biol. *129*, 1601–1615.

Wollert, T., Wunder, C., Lippincott-Schwartz, J., and Hurley, J. H. (2009). Membrane scission by the ESCRT-III complex. Nature *458*, 172–177.

Xiao, J., Chen, X. W., Davies, B. A., Saltiel, A. R., Katzmann, D. J., and Xu, Z. (2009). Structural basis of Ist1 function and Ist1-Did2 interaction in the multivesicular body pathway and cytokinesis. Mol. Biol. Cell *20*, 3514–3524.

Xiao, J., Xia, H., Zhou, J., Azmi, I. F., Davies, B. A., Katzmann, D. J., and Xu, Z. (2008). Structural basis of Vta1 function in the multivesicular body sorting pathway. Dev Cell *14*, 37–49.

Yeo, S. C., *et al*. (2003). Vps20p and Vta1p interact with Vps4p and function in multivesicular body sorting and endosomal transport in *Saccharomyces cerevisiae*. J. Cell Sci. *116*, 3957–3970.

Zamborlini, A., Usami, Y., Radoshitzky, S. R., Popova, E., Palu, G., and Gottlinger, H. (2006). Release of autoinhibition converts ESCRT-III components into potent inhibitors of HIV-1 budding. Proc. Natl. Acad. Sci. USA *103*, 19140–19145.